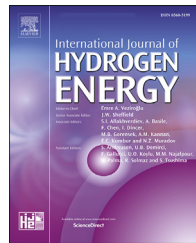




ELSEVIER

Available online at www.sciencedirect.com**ScienceDirect**journal homepage: www.elsevier.com/locate/he

Facile fabrication of a binary NiCo phosphide with hierarchical architecture for efficient hydrogen evolution reactions

Shijie Ma ^a, Lina Wang ^{a,*}, Songge Zhang ^a, Haonan Jin ^a, Meng Wan ^a,
Yi Pan ^a, Ting Zhang ^a, Yankun Wen ^a, Ming Zhang ^a, Han Zhu ^b,
Mingliang Du ^b

^a College of Materials and Textiles, Zhejiang Sci-Tech University, Hangzhou, 310018, PR China

^b Key Laboratory of Synthetic and Biological Colloids, Ministry of Education, School of Chemical and Material Engineering, Jiangnan University, Wuxi 214122, PR China

ARTICLE INFO

Article history:

Received 20 September 2018

Received in revised form

17 December 2018

Accepted 19 December 2018

Available online 18 January 2019

Keywords:

Binary NiCo phosphide

Hierarchical architecture

Electrocatalyst

HER

ABSTRACT

Exploring and designing efficient non-noble catalysts formed by element doping and nanostructure modification for the hydrogen evolution reaction (HER) is of critical importance with respect to sustainable resources. Herein, we have prepared a three-dimensional binary NiCo phosphide with hierarchical architecture (HA) composed of NiCoP nanosheets and nanowires grown on carbon cloth (CC) via a facile hydrothermal method followed by oxidation and phosphorization. Due to its unique hierarchical nanostructure, the NiCoP HA/CC electrocatalyst exhibits excellent performance and good working stability for the HER in both acidic and alkaline conditions. The obtained NiCoP HA/CC shows excellent HER activity with a low potential of 74 and 89 mV at 10 mA cm⁻², a small Tafel slope of 77.2 and 99.8 mV dec⁻¹ and long-term stability up to 24 h in acidic and alkaline electrolyte, respectively. NiCoP HA/CC, a non-noble metal material, is a promising electrocatalyst to replace noble metal-based electrocatalysts for the HER.

© 2019 Hydrogen Energy Publications LLC. Published by Elsevier Ltd. All rights reserved.

Introduction

Hydrogen has generally been considered to be one of the most promising sources of renewable energy given that traditional fossil fuel sources of energy are diminishing [1,2]. Electrochemical water splitting to produce hydrogen gas has attracted more attention due to the high efficiency, simplicity and environmental friendliness of the method [3–5]. In large-scale applications, the electrocatalyst plays a vital role in the

hydrogen evolution reaction (HER), since the electrocatalyst can significantly reduce the energy barrier and achieve favorable reaction efficiency [6–8]. Unfortunately, the rarity and high cost of noble metal-based catalysts limits their widespread application in electrochemical water splitting [9]. Therefore, earth-abundant transition metals (Fe, Co, Ni, Mo, V, etc.), and their chalcogenides [10–12], nitrides [13,14] and phosphides [15] have been widely explored to replace noble metal-based catalysts [16]. Among these alternative materials, transition-metal phosphides (TMPs) have attracted particular

* Corresponding author.

E-mail address: lnwang@zstu.edu.cn (L. Wang).

<https://doi.org/10.1016/j.ijhydene.2018.12.133>

0360-3199/© 2019 Hydrogen Energy Publications LLC. Published by Elsevier Ltd. All rights reserved.

attention due to the high catalytic activity originating from their hydrogenase-like catalytic mechanism [17,18]. However, the poor catalytic performance in alkaline media relative to that in acidic environments may be problematic for practical application because the oxygen evolution reaction (OER) often needs to be implemented in alkaline environments [19].

In the recent past, numerous studies have been performed to improve the electrocatalytic performance of TMPs in both acidic and alkaline conditions [20–22]. There are three major approaches to improve the HER activity of TMPs: (1) increasing the number of active sites on the catalyst, (2) improving the electrical conductivity of the catalyst, and (3) improving the catalytic effects of the active sites [23,24]. The performance of TMPs could be increased by metal doping [25–27]. Thus, compared with monometallic phosphides, bimetallic phosphides usually exhibit more abundant morphology and superior activity due to synergistic effects [28,29]. In addition, the regulation and control of the hierarchical architecture of the catalyst could effectively increase the number of active sites and further improve the electrical conductivity of the catalyst [30–32].

In this work, we describe a facile and effective method for fabricating binary NiCo phosphide with a unique three-

dimensional hierarchical architecture (NiCoP HA/CC) to serve as a highly efficient HER electrode material. The hierarchical architecture of the catalyst can be controlled by a hydrothermal process. The 3D NiCoP HA/CC can be directly used as an electrode for the HER. NiCoP HA/CC shows excellent HER activity and long-term stability up to 24 h, as well as a high cathodic current density in both acidic and alkaline electrolyte. The non-noble metal material NiCoP HA/CC is a promising electrocatalyst to replace noble metal-based electrocatalysts for HER.

Experiments

Preparation of NiCoP HA/CC

In a typical procedure, $\text{Ni}(\text{NO}_3)_2 \cdot 6\text{H}_2\text{O}$ (1.5 mmol), $\text{Co}(\text{NO}_3)_2 \cdot 6\text{H}_2\text{O}$ (1.5 mmol), $\text{CO}(\text{NH}_2)_2$ (15 mmol) and NH_4F (8 mmol) were dissolved in 30 mL of distilled water and stirred to form a homogeneous solution. A piece of carbon cloth (CC) (2 cm × 3 cm) was pretreated by nitric acid for 2 h and then ultrasonically cleaned with alcohol and deionized water for 10 min in sequence. The solution and CC were transferred into

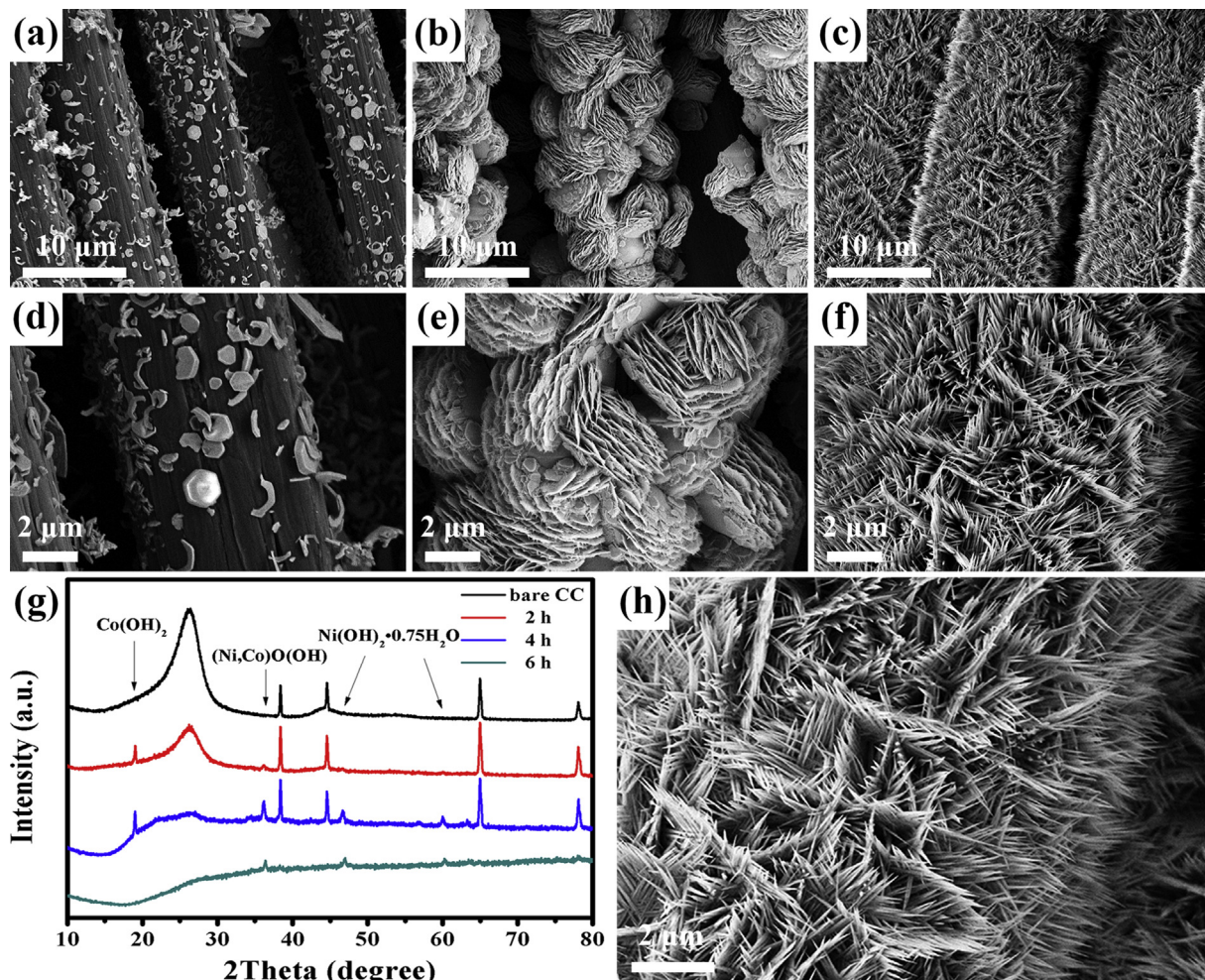


Fig. 1 – SEM images of the NiCo precursor obtained at different reaction times: (a, d) 2 h, (b, e) 4 h, (c, f) 6 h. (g) XRD patterns of bare CC and the NiCo precursor obtained at different reaction times. (h) SEM image of NiCoP HA/CC.

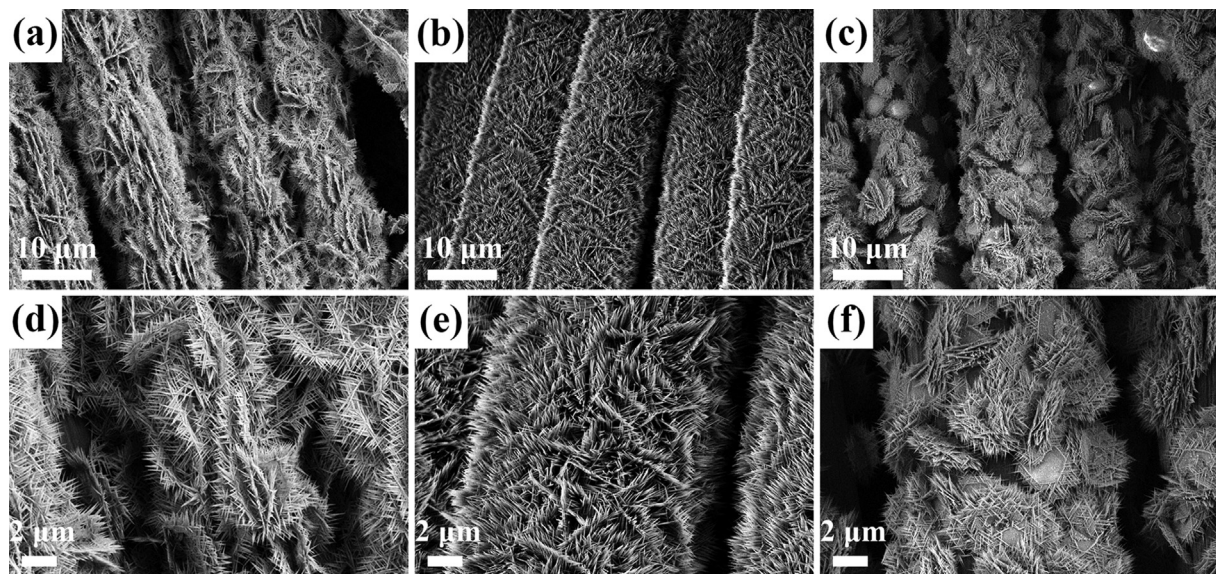


Fig. 2 – SEM images of NiCo precursor synthesized with different contents of NH_4F : (a, d) 4, (b, e) 8, (c, f) 12 mmol.

a 50 ml Teflon-lined stainless autoclave, which was sealed and maintained at 120 °C for 6 h in an oven and then cooled down to room temperature naturally. The NiCo precursor was taken out and washed with deionized water before being dried at 60 °C. After this, the NiCo precursor was calcined at 450 °C for 2 h to ensure good crystallinity and close contact between the sample and the substrate. The as-prepared NiCoO precursor and 0.5 g NaH_2PO_2 were placed separately in a porcelain boat before being heated in a tube furnace at 300 °C for 2 h under Ar flow. After washing with deionized water, the as-prepared NiCoP HA/CC was dried at 60 °C.

The hierarchical architecture was constructed by regulating the content of NH_4F and the reaction time of the hydrothermal process. The products with different reaction time (2 h, 4 h and 6 h) and content of NH_4F (4 mmol, 8 mmol and 12 mmol) were synthesized and investigated.

For comparison, $\text{Co}_2\text{P}/\text{CC}$ and $\text{Ni}_2\text{P}/\text{Ni}_5\text{P}_4/\text{CC}$ were prepared in a similar way without adding $\text{Ni}(\text{NO}_3)_2 \cdot 6\text{H}_2\text{O}$ or $\text{Co}(\text{NO}_3)_2 \cdot 6\text{H}_2\text{O}$, respectively. NiCoP/CC (2:1) and NiCoP/CC (1:2) were fabricated in the same way using different initial molar ratios of $\text{Ni}(\text{NO}_3)_2 \cdot 6\text{H}_2\text{O}$ to $\text{Co}(\text{NO}_3)_2 \cdot 6\text{H}_2\text{O}$, namely, 2:1 and 1:2, respectively.

Instruments

The morphology and structure of the samples were characterized using field-emission scanning electron microscopy (FE-SEM, ULTRA55, Zeiss, Germany) and transmission electron microscopy (TEM, JEM-2100, JOEL, Japan) at the acceleration voltage of 200 kV. Phase analysis of the samples was performed by X-ray diffractometer (XRD, Bruker AXS8 DISCOVER). The X-ray photoelectron spectroscopy (XPS) measurements were recorded with an X-ray photoelectron spectrometer (Kratos Axis Ultra DLD) using a monochromatic Al K_α source (1486.6 eV). High-angle annular dark-field scanning TEM (HAADF-STEM) images, STEM mapping and line-scan energy dispersive X-ray spectroscopy (EDX) spectra were recorded by an STEM (Tecnai G2 F30S-Twin, Philips-FEI) at an acceleration voltage of 300 kV.

Electrochemical characterization

All electrochemical experiments were carried out using an electrochemical analyzer (IviumStat.h, Ivium Tech, Netherlands) with a standard three-electrode cell testing

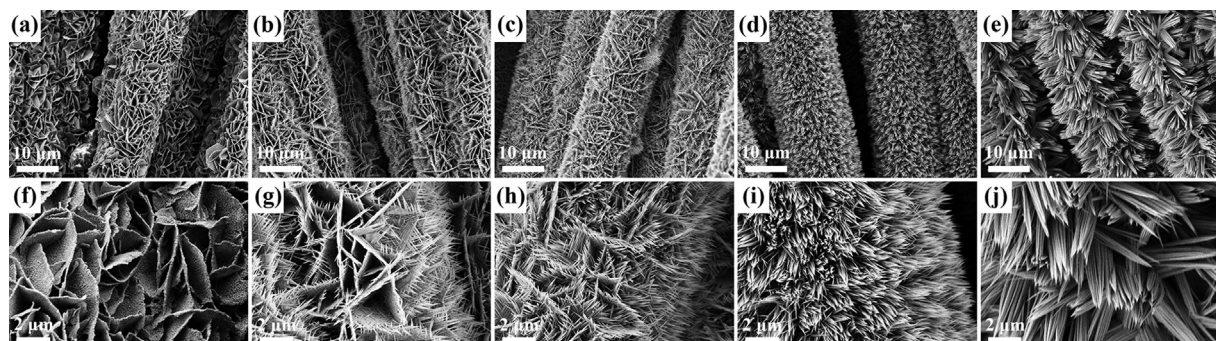


Fig. 3 – SEM images of (a, f) $\text{Ni}_2\text{P}/\text{Ni}_5\text{P}_4/\text{CC}$, (b, g) NiCoP/CC (2:1), (c, h) NiCoP HA/CC, (d, i) NiCoP/CC (1:2), and (e, j) $\text{Co}_2\text{P}/\text{CC}$.

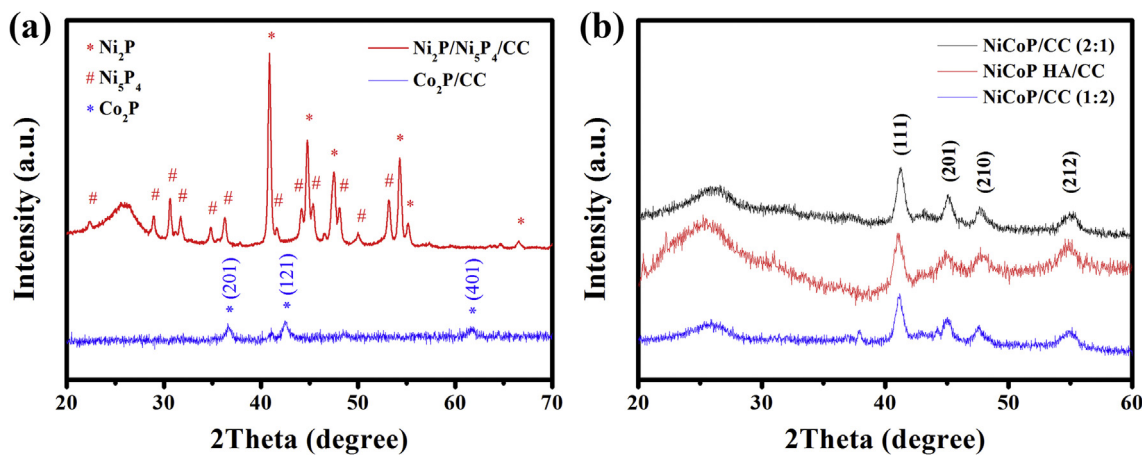


Fig. 4 – (a) XRD patterns of $\text{Ni}_2\text{P}/\text{Ni}_5\text{P}_4/\text{CC}$ and $\text{Co}_2\text{P}/\text{CC}$. **(b)** XRD patterns of NiCoP/CC (2:1), $\text{NiCoP HA}/\text{CC}$ and NiCoP/CC (1:2).

system at room temperature. A graphite rod and a saturated calomel electrode were used as the counter and reference electrodes, respectively. Electrochemical characterization was performed in an aqueous solution of 0.5 M H_2SO_4 or 1 M KOH. Prior to data collection, the working electrodes were preprocessed under a continuous Ar flow by cyclic voltammetry to bubble away the surface contaminants. The potentials were calibrated against a reversible hydrogen electrode (RHE).

Results and discussion

The binary NiCo phosphide hierarchical architecture grown on CC ($\text{NiCoP HA}/\text{CC}$) was prepared by a hydrothermal method and an oxidation process, followed by low-temperature phosphorization using NaH_2PO_2 as a P source. Reaction time of the hydrothermal process directly affects the construction of hierarchical architecture. A time-dependent experiment

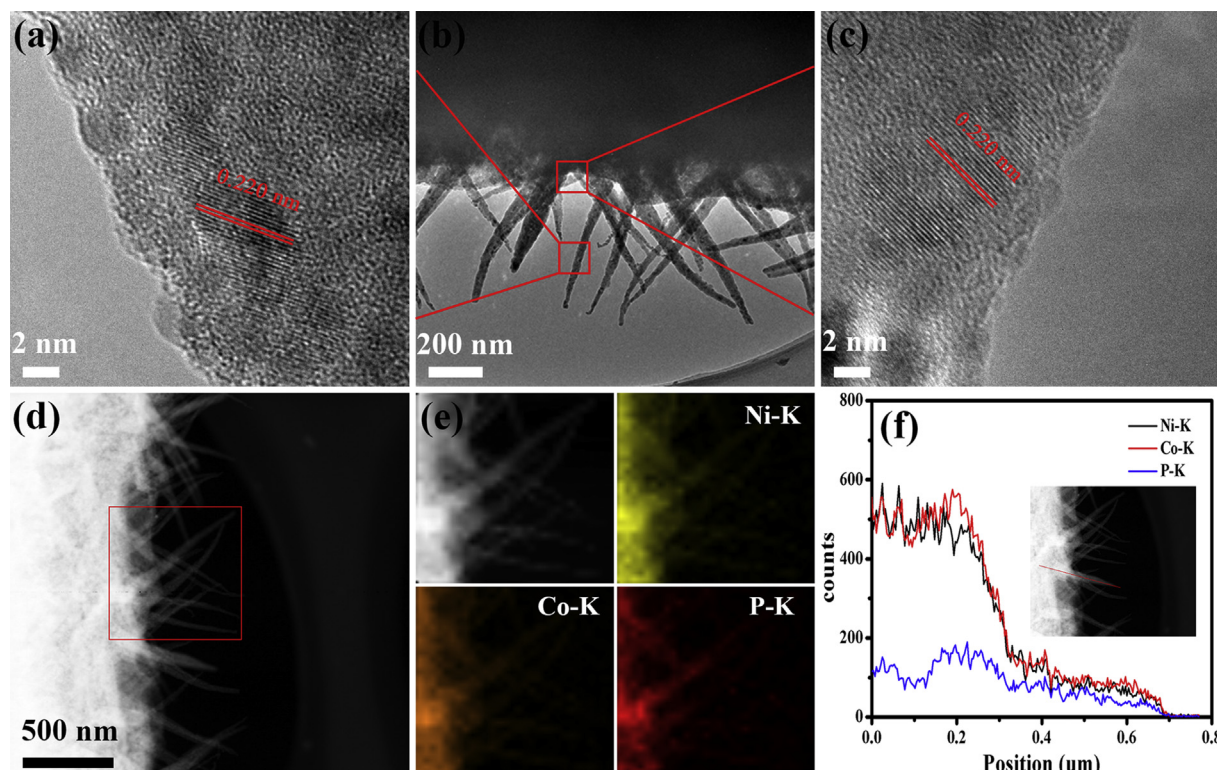


Fig. 5 – (a) HRTEM of NiCoP nanowire, **(b)** TEM of NiCoP HA and **(c)** NiCoP nanosheet on NiCoP HA . **(d)** HAADF-STEM and **(e)** STEM-EDX mapping images of NiCoP HA . **(f)** Line-scan EDX spectra of NiCoP HA .

was firstly performed to investigate the evolution of the hydrothermal process. Fig. 1a–g shows the scanning electron microscopy (SEM) images and X-ray diffraction (XRD) patterns of NiCo precursors obtained at different reaction times of 2 h, 4 h and 6 h. Before 2 h, a few scattered sheets started to grow on the carbon cloth (Fig. 1a, d), and the major phase was Co(OH)_2 (red line in Fig. 1g). At 4 h, the carbon cloth was covered with multidirectional nanosheets, and several burr-like nanowires were observed on the nanosheets (Fig. 1b, e). The diffraction peaks of $(\text{Ni},\text{Co})\text{O}(\text{OH})$ and $\text{Ni(OH)}_2 \cdot 0.75\text{H}_2\text{O}$ appeared at this time, coexisting with Co(OH)_2 (blue line in Fig. 1g). When the reaction time reached 6 h, numerous nanowires had grown along the direction of the growth of the nanosheets to finally form a hierarchical architecture (Fig. 1c, f). The diffraction peaks of Co(OH)_2 disappeared, and the major phases were $(\text{Ni},\text{Co})\text{O}(\text{OH})$ and $\text{Ni(OH)}_2 \cdot 0.75\text{H}_2\text{O}$ (green line in Fig. 1g). By controlling the reaction time of the hydrothermal process, the morphology of the NiCo precursor changed from a single structure to hierarchical architecture. Moreover, the NiCoP HA/CC materials retained their morphology well after oxidation and phosphorization (Fig. 1h).

In hydrothermal experiments, the content of NH_4F in solution plays a very important role in the regulation and control of hierarchical architecture. To further investigate the detailed formation mechanism, we carefully studied the effects of different NH_4F contents at 4 mmol, 8 mmol and 12 mmol on morphology. Fig. 2 shows the morphology of the

NiCo precursors obtained under various contents of NH_4F . When the content of NH_4F was 8 mmol, forest-like NiCo HA nanowire was clearly obtained (Fig. 2b, e). However, at 4 mmol, the density of the nanowire on CC increased with a lower content of NH_4F (Fig. 2a, d). As the content increased to 12 mmol, the bunched NiCo nanowires tended to assemble into nanosheet-like structures (Fig. 2c, f). In the reaction process, the morphology of the product strongly depends on the growth kinetics and the regulating effect of NH_4F is mainly attributed to F^- . Owing to the hydrolysis of F^- [33], the combination of F^- and H_2O reduces the concentration of water molecules. This effect inhibits the movement of water molecules and leads to an increase in the average activity coefficient of ions in solution. The result is an increase in reaction rate and a rapid build-up of product particles. Besides, F^- can adsorb on the surface of the primary particles, hinder the orderly growth of the particles, and eventually make them grow disorderly in many directions into a higher dimensional structure [34].

Based on the experimental results and discussions, we can draw the conclusion: the content of NH_4F plays an important role in the formation of hierarchical structure. At the beginning of hydrothermal reaction, higher amounts of NH_4F could lead to the growth of two-dimensional nanosheet-like NiCo bunched nanowires on CC in aqueous solution. As the reaction continued, $\text{CO}(\text{NH}_2)_2$ and metal salts were gradually consumed. Low reaction rate promoted the growth of

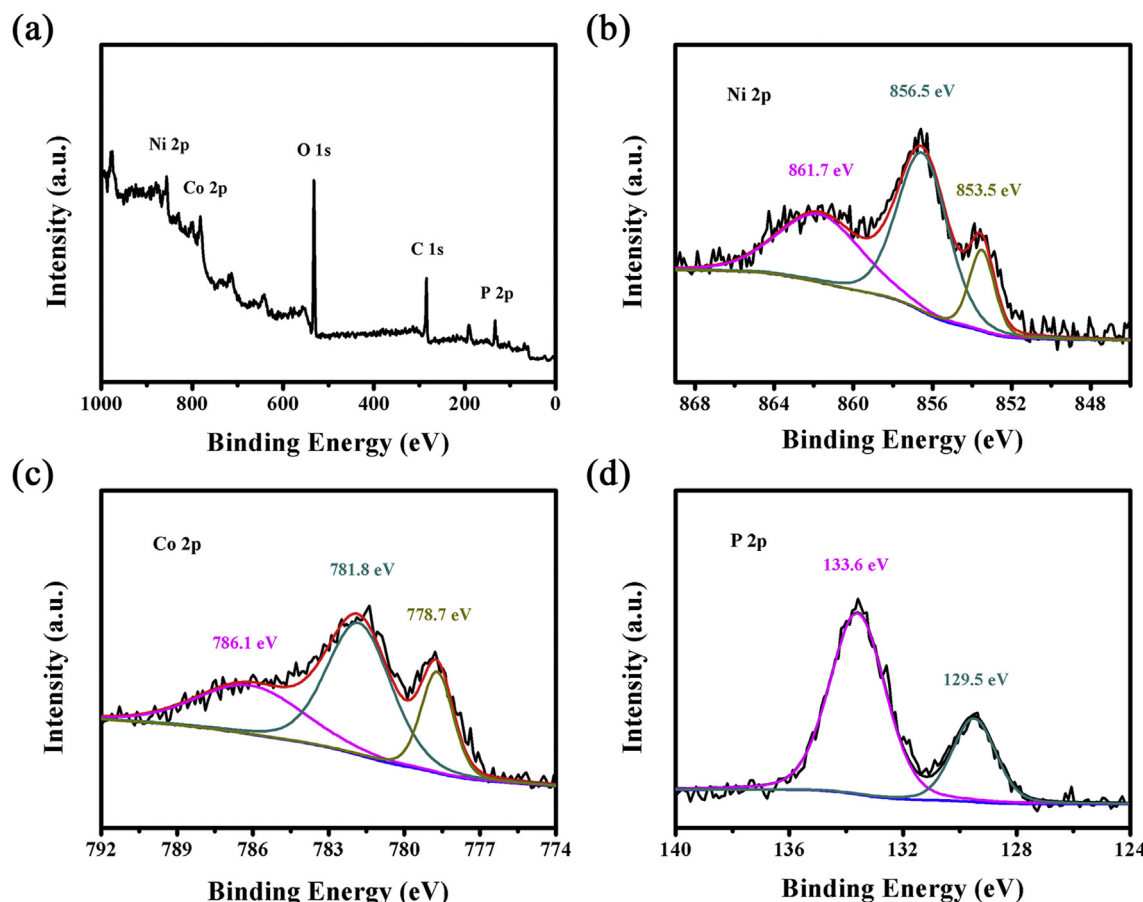


Fig. 6 – XPS spectra of NiCoP HA/CC: (a) survey, (b) Ni 2p, (c) Co 2p and (d) P 2p regions.

nanowires and loading on nanosheets, resulting in the formation of NiCo HA structures.

To obtain the optimal ratio of metal salts, we fabricated contrasting samples in the same way using different initial molar ratios of metal salts. The surface morphology of the different as-prepared samples was characterized by SEM. As shown in Fig. 3, $\text{Ni}_2\text{P}/\text{Ni}_5\text{P}_4/\text{CC}$ nanosheets, NiCoP HA (2:1), NiCoP nanowire arrays (1:2) and Co_2P nanowire arrays were grown on CC. The successful formation of TMPs after subsequent two-step posttreatment was confirmed by XRD analysis. Fig. 4b shows the XRD patterns of NiCoP HA/CC and contrasting samples fabricated in the same way using different initial molar ratios of metal salts. The characteristic peaks at 41.0° , 44.9° , 47.6° and 75.4° can be indexed to the (111), (201), (210) and (212) planes of NiCoP (JCPDS No. 71-2336), respectively. Fig. 4a presents the XRD patterns of two monometallic phosphides grown on CC. The $\text{Co}_2\text{P}/\text{CC}$ exhibits three main characteristic peaks, indexed to the (201), (121) and (401) planes of Co_2P (JCPDS No. 74-0287). The XRD pattern of $\text{Ni}_2\text{P}/\text{Ni}_5\text{P}_4/\text{CC}$ is in good accordance with the standard Ni_2P (JCPDS 03-0953) and the standard Ni_5P_4 (JCPDS 18-0883).

The TEM image in Fig. 5b further shows multilayer NiCoP nanosheets and connected nanosheets and nanowires, which is consistent with the results of SEM. Fig. 5a and c presents

high-resolution transmission electron microscope (HRTEM) images of a typical nanowire and nanosheet, indicating high-quality crystallinity with lattice fringes of 0.220 nm, which is in good agreement with (111) lattice planes. To unambiguously determine the distribution of elements, we employed elemental mapping by scanning transmission electron microscopy (STEM). High-resolution EDX elemental mapping images are shown in Fig. 5e. This confirms the homogeneous distribution of Ni, Co and P elements, and a high spatial correlation is presented over the entire mapped area. Line-scan EDX spectra extending across NiCoP nanosheets along NiCoP nanowires in the selected region are shown in Fig. 5f. The spectra indicate that the Ni, Co and P elements are concomitant in the nanowire while the P element is relatively scarce in the nanosheet. Combined with the above characterization, we conclude that the component of the nanowire and the surface of nanosheets is NiCoP, which formed during phosphating process and contributed to catalysis for hydrogen evolution reaction.

X-ray photoelectron spectroscopy (XPS) analysis was then utilized to probe the surface chemistry of NiCoP HA/CC. As shown by the XPS survey spectra in Fig. 6a, Ni, Co, P, C, and O coexisted in the as-prepared NiCoP HA/CC. Fig. 6b–d displays high-resolution spectra of the Co 2p, Ni 2p, and P 2p core

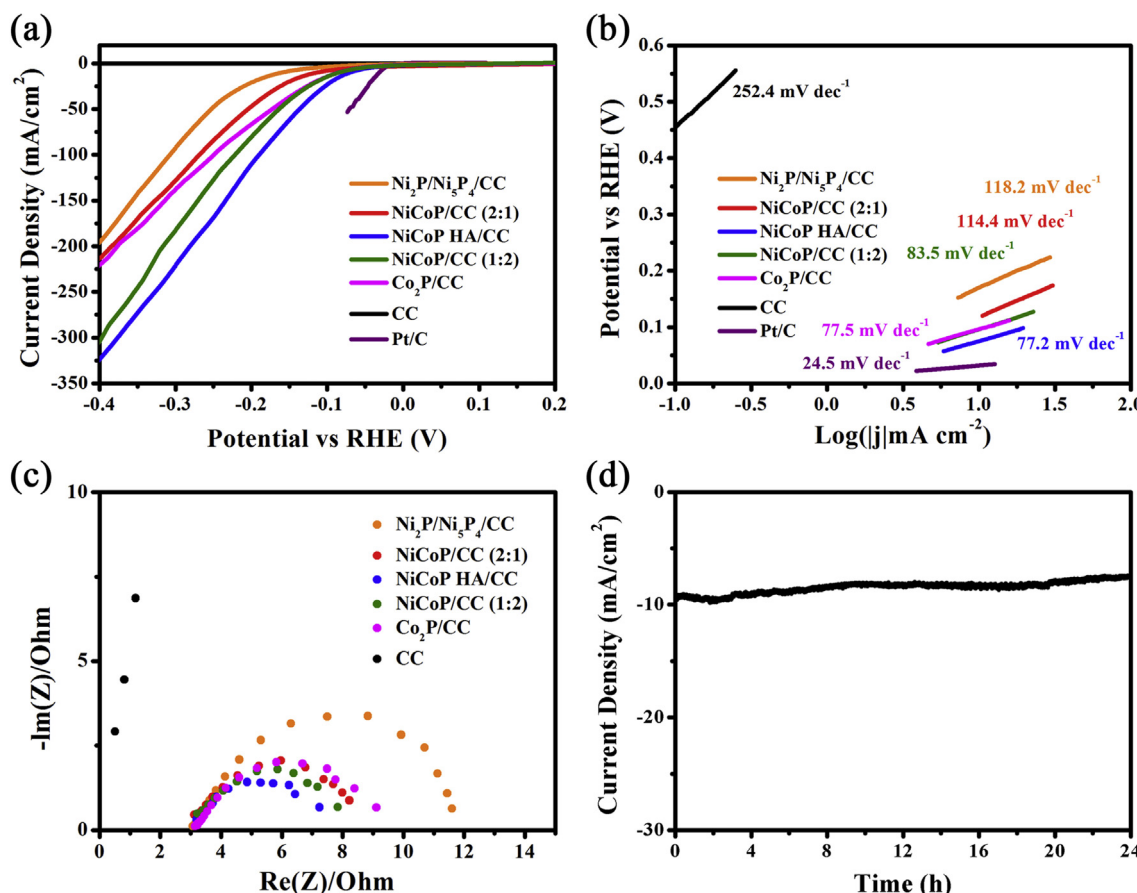


Fig. 7 – Hydrogen evolution reaction electrocatalysis in 0.5 M H_2SO_4 . (a) LSV curves of HER, (b) corresponding Tafel plots and (c) electrochemical impedance spectra at $\eta = 100 \text{ mV}$ of NiCoP HA/CC, along with Pt/C, $\text{Ni}_2\text{P}/\text{Ni}_5\text{P}_4/\text{CC}$, NiCoP/CC (2:1), NiCoP/CC (1:2), $\text{Co}_2\text{P}/\text{CC}$ and CC for comparison. (d) Time-dependent current density of NiCoP HA/CC at a constant voltage of -74 mV vs. RHE.

levels. In the high-resolution Ni 2p region (Fig. 6b), the peaks at 853.5 and 865.6 eV are attributed to Ni 2p_{3/2}, while the peak at 861.7 eV belongs to the satellite of the Ni 2p_{3/2} peak. In the Co 2p spectrum (Fig. 6c), the peaks at 778.7 and 781.8 eV are attributed to Co 2p_{3/2}, while the peak at 786.1 belongs to the satellite of the Co 2p_{3/2} peak. For Co 2p_{3/2}, the peak located at 778.7 eV is assigned to Co–P. The peak at 781.8 eV can be ascribed to an oxidized state of Co [17]. The high-resolution P 2p spectrum (Fig. 6d) shows two peaks at 129.5 and 133.6 eV. The peaks at 853.5 eV for Ni 2p_{3/2}, 778.7 eV for Co 2p_{3/2} and 129.5 eV for P 2p_{3/2} are associated with the typical binding energies for Ni 2p, Co 2p and P 2p contributions in NiCoP, respectively [18]. All of the above characterizations and analyses confirm the successful conversion of the NiCo precursor to NiCoP HA on CC.

Subsequently, the electrochemical performance of NiCoP HA/CC towards HER was investigated using a typical three-electrode cell testing system in both acid (0.5 M H₂SO₄) and alkaline (1.0 M KOH) conditions. NiCoP HA/CC was directly used as the working electrode. A graphite rod and a saturated calomel electrode were used as the counter and reference electrodes, respectively. Fig. 7a shows the LSV curves of the HER in 0.5 M H₂SO₄ catalyzed by various catalysts. Among the considered catalysts, NiCoP HA/CC had a low overpotential of

74 mV at the current density of 10 mA cm⁻², close to the value of 20% Pt/C and much lower than those of Ni₂P/Ni₅P₄/CC (170 mV), NiCoP/CC (2:1) (118 mV), NiCoP/CC (1:2) (96 mV) and Co₂P/CC (97 mV). For further insight into the catalytic kinetics and intrinsic properties of the electrocatalysts, Tafel plots (Fig. 7b) were fitted to the Tafel equation ($\eta = b \log(j) + a$). The results indicate that the Tafel slope of NiCoP HA/CC (77.2 mV dec⁻¹) was close to that of 20% Pt/C (24.5 mV dec⁻¹). In addition to electrochemical performance, enhanced charge transfer kinetics contribute to the improved HER efficiency of a catalyst. We evaluated the AC impedance at an overpotential of 100 mV (Fig. 7c). NiCoP HA/CC exhibits a smaller charge transfer impedance (4.2 Ohm) than that of Ni₂P/Ni₅P₄/CC (9.1 Ohm), NiCoP/CC (2:1) (5.4 Ohm), NiCoP/CC (1:2) (5.0 Ohm) and Co₂P/CC (5.8 Ohm), suggesting a faster electron transfer rate for the HER with NiCoP HA/CC. In addition to catalytic activity, durability and long-term stability, especially at high current density, are essential qualities for an advanced electrocatalyst. A chronoamperometry test demonstrated that NiCoP HA/CC works efficiently for more than 24 h (Fig. 7d) at a high current density of 10 mA cm⁻².

In 1.0 M KOH (as shown in Fig. 8a), a small overpotential of 89 mV for NiCoP HA/CC can lead to a current density of 10 mA cm⁻², which is slightly higher than that of 20% Pt/C

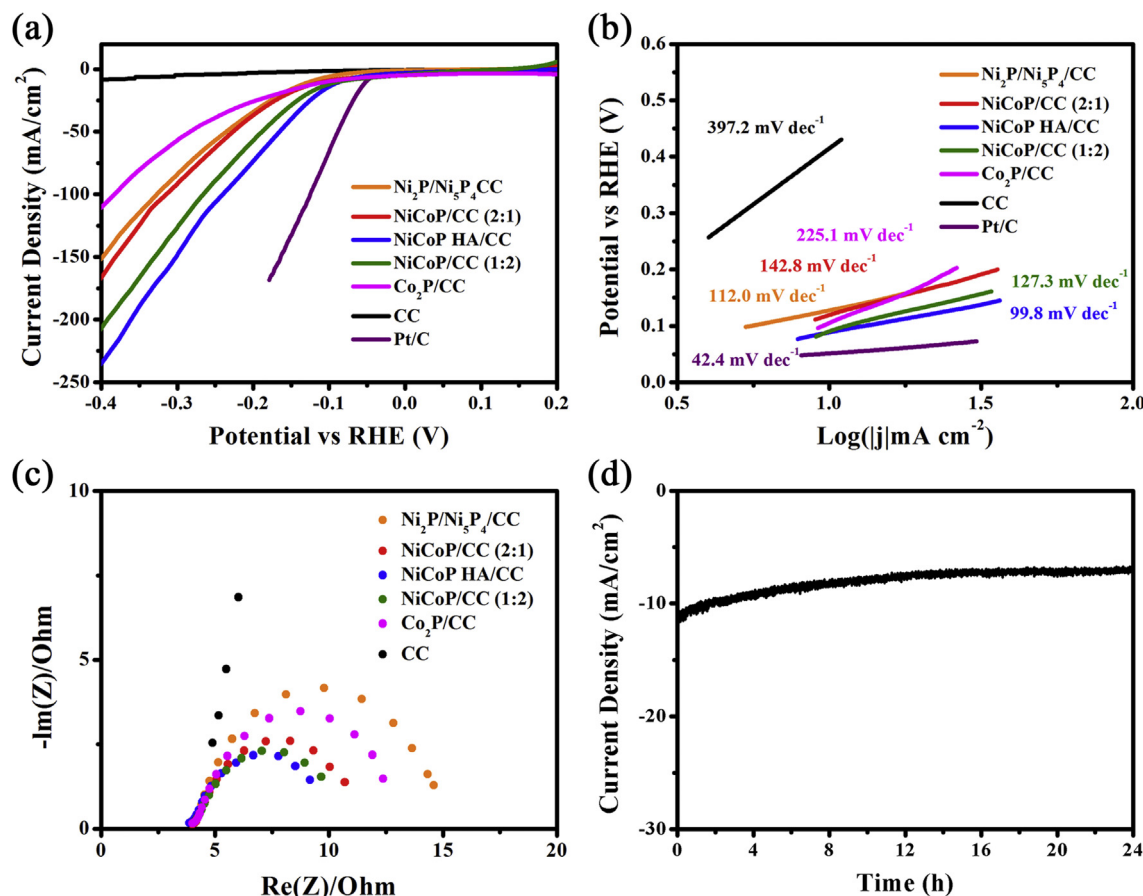


Fig. 8 – Hydrogen evolution reaction electrocatalysis in 1 M KOH. (a) LSV curves of HER, (b) corresponding Tafel plots and (c) electrochemical impedance spectra at $\eta = 100$ mV vs. RHE of NiCoP HA/CC, along with Pt/C, Ni₂P/Ni₅P₄/CC, NiCoP/CC (2:1), NiCoP/CC (1:2), Co₂P/CC and CC for comparison. (d) Time-dependent current density of NiCoP HA/CC at a constant voltage of -89 mV vs. RHE.

(52 mV) and much lower than those of the other compared electrocatalysts. Moreover, the small Tafel slope (99.8 mV dec⁻¹) of NiCoP HA/CC is comparable with that of 20% Pt/C (Fig. 8b). Fig. 8c displays the electrochemical impedance spectra. Clearly, the resistance of NiCoP HA/CC is much smaller, and the charge transfer resistance (R_{ct}) of NiCoP HA/CC is only 5.7 Ohm. Similarly, the Tafel slope and electrochemical impedance values are both significantly superior to those of various TMP-based HER electrocatalysts (Fig. 8b and c). The smaller Tafel slope and electrochemical impedance of NiCoP HA/CC reveal that this material possesses faster HER kinetics than do the other electrocatalysts in alkaline media. Time-dependent current density analysis showed only a small degradation in the current density after 24 h (Fig. 8d), indicating the strong stability of NiCoP HA/CC.

Conclusions

In summary, we have successfully designed and synthesized a 3D self-supported NiCoP HA/CC that can serve as an efficient HER electrocatalyst in both acidic and alkaline conditions. NiCoP HA/CC was prepared via a facile hydrothermal method followed by oxidation and phosphorization. A unique hierarchical architecture was constructed by controlling the optimal ratio of metal salts, the content of NH₄F and the reaction time of the hydrothermal process. The obtained NiCoP HA/CC shows excellent HER activity with a low potential of 74 and 89 mV at 10 mA cm⁻², a small Tafel slope of 77.2 and 99.8 mV dec⁻¹ and long-term stability up to 24 h in acidic and alkaline electrolyte, respectively. This work demonstrates that NiCoP HA/CC with a unique three-dimensional hierarchical architecture is a promising substitute for noble metal-based materials in large-scale electrochemical water splitting. Moreover, hierarchical architecture is likely to be applied in other fields of electrochemistry, such as lithium-ion batteries and supercapacitors.

R E F E R E N C E S

- [1] Zhang R, Wang X, Yu S, Wen T, Zhu X, Yang F, Sun X, Wang X, Hu W. Ternary NiCo_{2-x} nanowires as pH-Universal electrocatalysts for highly efficient hydrogen evolution reaction. *Adv Mater* 2017;29:1605502.
- [2] Li J, Wei G, Zhu Y, Xi Y, Pan X, Ji Y, Zatovsky IV, Han W. Hierarchical NiCoP nanocone arrays supported on Ni foam as an efficient and stable bifunctional electrocatalyst for overall water splitting. *J Mater Chem* 2017;5:14828–37.
- [3] Wang J, Zhu H, Chen J, Zhang B, Zhang M, Wang L, Du M. Small and well-dispersed Cu nanoparticles on carbon nanofibers: self-supported electrode materials for efficient hydrogen evolution reaction. *Int J Hydrogen Energy* 2016;41:18044–9.
- [4] Zhong X, Tang J, Wang J, Shao M, Chai J, Wang S, Yang M, Yang Y, Wang N, Wang S, Xu B, Pan H. 3D heterostructured pure and N-Doped Ni₃S₂/VS₂ nanosheets for high efficient overall water splitting. *Electrochim Acta* 2018;269:55–61.
- [5] Ai L, Niu Z, Jiang J. Mechanistic insight into oxygen evolution electrocatalysis of surface phosphate modified cobalt phosphide nanorod bundles and their superior performance for overall water splitting. *Electrochim Acta* 2017;242:355–63.
- [6] Lin Y, Pan Y, Zhang J. CoP nanorods decorated biomass derived N, P co-doped carbon flakes as an efficient hybrid catalyst for electrochemical hydrogen evolution. *Electrochim Acta* 2017;232:561–9.
- [7] Wu J, Ge X, Li Z, Cao D, Xiao J. Highly dispersed NiCoP nanoparticles on carbon nanotubes modified nickel foam for efficient electrocatalytic hydrogen production. *Electrochim Acta* 2017;252:101–8.
- [8] Wang XD, Chen HY, Xu YF, Liao JF, Chen BX, Rao HS, Kuang DB, Su CY. Self-supported NiMoP₂ nanowires on carbon cloth as an efficient and durable electrocatalyst for overall water splitting. *J Mater Chem* 2017;5:7191–9.
- [9] Pu Z, Zhang C, Amiinu IS, Li W, Wu L, Mu S. General strategy for the synthesis of transition-metal phosphide/N-doped carbon frameworks for hydrogen and oxygen evolution. *ACS Appl Mater Interfaces* 2017;9:16187–93.
- [10] Zhang J, Zhang C, Wang Z, Zhu J, Wen Z, Zhao X, Zhang X, Xu J, Lu Z. Synergistic interlayer and defect engineering in VS₂ nanosheets toward efficient electrocatalytic hydrogen evolution reaction. *Small* 2018;14:1703098.
- [11] Yang Y, Zhang K, Lin H, Li X, Chan HC, Yang L, Gao Q. MoS₂–Ni₃S₂ heteronanoarods as efficient and stable bifunctional electrocatalysts for overall water splitting. *ACS Catal* 2017;7:2357–66.
- [12] Luo P, Zhang H, Liu L, Zhang Y, Deng J, Xu C, Hu N, Wang Y. Targeted synthesis of unique nickel sulfide (NiS, NiS₂) microarchitectures and the applications for the enhanced water splitting system. *ACS Appl Mater Interfaces* 2017;9:2500–8.
- [13] Yin Z, Sun Y, Zhu C, Li C, Zhang X, Chen Y. Bimetallic Ni–Mo nitride nanotubes as highly active and stable bifunctional electrocatalysts for full water splitting. *J Mater Chem* 2017;5:13648–58.
- [14] Balogun MS, Huang Y, Qiu W, Yang H, Ji H, Tong Y. Updates on the development of nanostructured transition metal nitrides for electrochemical energy storage and water splitting. *Mater Today* 2017;20:425–51.
- [15] Peng W, Jiao L, Huan Q, Li L, Yang J, Zhao Q, Wang Q, Du H, Liu G, Si Y, Wang Y, Yuan H. Co₂P: a facile solid state synthesis and its applications in alkaline rechargeable batteries. *J Alloy Comp* 2012;511:198–201.
- [16] Yan XY, Devaramani S, Chen J, Shan DL, Qin DD, Ma Q, Lu XQ. Self-supported rectangular CoP nanosheet arrays grown on a carbon cloth as an efficient electrocatalyst for the hydrogen evolution reaction over a variety of pH values. *New J Chem* 2017;41:2436–42.
- [17] Du C, Yang L, Yang F, Cheng G, Luo W. Nest-like NiCoP for highly efficient overall water splitting. *ACS Catal* 2017;7:4131–7.
- [18] Li Y, Zhang H, Jiang M, Kuang Y, Sun X, Duan X. Ternary NiCoP nanosheet arrays: an excellent bifunctional catalyst for alkaline overall water splitting. *Nano Research* 2016;9:2251–9.
- [19] Li G, Zhang D, Yu Y, Huang S, Yang W, Cao L. Activating MoS₂ for pH-Universal hydrogen evolution catalysis. *J Am Chem Soc* 2017;139:16194–200.
- [20] Pu Z, Xue Y, Li W, Amiinu IS, Mu S. Efficient water splitting catalyzed by flexible NiP₂ nanosheet array electrodes under both neutral and alkaline solutions. *New J Chem* 2017;41:2154–9.
- [21] Teng Y, Wang XD, Chen HY, Liao JF, Li WG, Kuang DB. Iron-assisted engineering of molybdenum phosphide nanowires on carbon cloth for efficient hydrogen evolution in a wide pH range. *J Mater Chem* 2017;5:22790–6.
- [22] Lv Y, Wang X. Nonprecious metal phosphides as catalysts for hydrogen evolution, oxygen reduction and evolution reactions. *Catalysis Science & Technology* 2017;7:3676–91.

- [23] Yang H, Zhang T, Zhu H, Zhang M, Wu W, Du M. Synthesis of a $\text{MoS}_{2(1-x)}\text{Se}_{2x}$ ternary alloy on carbon nanofibers as the high efficient water splitting electrocatalyst. *Int J Hydrogen Energy* 2017;42:1912–8.
- [24] Jiang P, Liu Q, Sun X. NiP_2 nanosheet arrays supported on carbon cloth: an efficient 3D hydrogen evolution cathode in both acidic and alkaline solutions. *Nanoscale* 2014;6:13440–5.
- [25] Pei Y, Yang Y, Zhang F, Dong P, Baines R, Ge Y, Chu H, Ajayan PM, Shen J, Ye M. Controlled electrodeposition synthesis of Co-Ni-P Film as a flexible and inexpensive electrode for efficient overall water splitting. *ACS Appl Mater Interfaces* 2017;9:31887–96.
- [26] Liu S, Liu Q, Lv Y, Chen B, Zhou Q, Wang L, Zheng Q, Che C, Chen C. Ru decorated with NiCoP: an efficient and durable hydrogen evolution reaction electrocatalyst in both acidic and alkaline conditions. *Chem Commun* 2017;53:13153–6.
- [27] Ray C, Lee SC, Jin B, Kundu A, Park JH, Jun SC. Stacked porous iron-doped nickel cobalt phosphide nanoparticle: an efficient and stable water splitting electrocatalyst. *ACS Sustainable Chem Eng* 2018;6:6146–56.
- [28] Ahn SH, Manthiram A. Direct growth of ternary Ni–Fe–P porous nanorods onto nickel foam as a highly active, robust bi-functional electrocatalyst for overall water splitting. *J Mater Chem* 2017;5:2496–503.
- [29] Wang P, Pu Z, Li Y, Wu L, Tu Z, Jiang M, Kou Z, Amiuu IS, Mu S. Iron-doped nickel phosphide nanosheet arrays: an efficient bifunctional electrocatalyst for water splitting. *ACS Appl Mater Interfaces* 2017;9:26001–7.
- [30] Chen X, Chen D, Guo X, Wang R, Zhang H. Facile growth of caterpillar-like NiCo_2S_4 nanocrystal arrays on nickle foam for high-performance supercapacitors. *ACS Appl Mater Interfaces* 2017;9:18774–81.
- [31] Wang Z, Zeng S, Liu W, Wang X, Li Q, Zhao Z, Geng F. Coupling molecularly ultrathin sheets of NiFe-layered double hydroxide on NiCo_2O_4 nanowire arrays for highly efficient overall water-splitting activity. *ACS Appl Mater Interfaces* 2017;9:1488–95.
- [32] Ma X, Chang Y, Zhang Z, Tang J. Forest-like $\text{NiCoP}@\text{Cu}_3\text{P}$ supported on copper foam as a bifunctional catalyst for efficient water splitting. *J Mater Chem* 2018;6:2100–6.
- [33] Zeng S, Tang R, Duan S, Li L, Liu C, Gu X, Wang S, Sun D. Kinetically controlled synthesis of bismuth tungstate with different structures by a NH_4F assisted hydrothermal method and surface-dependent photocatalytic properties. *J Colloid Interface Sci* 2014;432:236–45.
- [34] Turgut G, Sonmez E, Aydin S, Dilber R, Turgut U. The effect of Mo and F double doping on structural, morphological, electrical and optical properties of spray deposited SnO_2 thin films. *Ceram Int* 2014;40:12891–8.